arXiv:1702.02829v1 [cond-mat.mes-hall] 9 Feb 2017

Hyperbolic cooling of a graphene on hBN transistor in the Zener-Klein regime.

W. Yang,[1] S. Berthou,[1] X. Lu,[2] Q. Wilmart,[1] A. Denis,[1] M. Rosticher,[3] T. Taniguchi,[4] K. Watanabe,[4] G. Fève,[1] J.M. Berroir,[1] G. Zhang,[2] C. Voisin,[1] E. Baudin,[1] and B. Plaçais[1,*]

[1]*Laboratoire Pierre Aigrain, École Normale Supérieure, PSL Research University, CNRS, Université Pierre et Marie Curie, Sorbonne Universités, Université Paris Diderot, Sorbonne Paris-Cité, 24 rue Lhomond, 75231 Paris Cedex 05, France*

[2]*Beijing National Laboratory for Condensed Matter Physics and Institute of Physics, Chinese Academy of Sciences, Beijing 100190, China*

[3]*Département de Physique, École Normale Supérieure-PSL Research University, CNRS, Université Pierre et Marie Curie-Sorbonne Universités, Université Paris Diderot-Sorbonne Paris Cité, 24 rue Lhomond, 75231 Paris Cedex 05, France*

[4]*Advanced Materials Laboratory, National Institute for Materials Science, Tsukuba, Japan*

(Dated: February 10, 2017)

Engineering of cooling mechanisms is a bottleneck in nanoelectronics. Whereas thermal exchanges in diffusive graphene are driven by defect assisted acoustic phonon scattering (the so-called supercollisions), the case of high-mobility graphene on hexagonal Boron Nitride (hBN) is radically different with a prominent contribution of remote phonons from the substrate. Here, we show that a bi-layer graphene on hBN transistor with local gate can be driven in a very original regime where almost perfect current saturation is achieved by compensation of the decrease of the carrier density and Zener-Klein tunneling (ZKT) at high bias, leading to unprecedented figures for the voltage gain. Using noise thermometry, we show that this Zener-Klein tunneling triggers a new cooling pathway due to the emission of hyperbolic phonons (HPP) in hBN by out-of-equilibrium electron-hole pairs beyond the super-Planckian regime. The combination of ZKT-transport and HPP-cooling promotes graphene on BN transistors as a valuable nanotechnology for power devices and RF electronics.

Energy relaxation in solids is provided by electron-electron interactions and phonon emission. The former give rise to Wiedemann-Franz (WF) heat conduction to the leads. In diffusive graphene, the latter is dominated by three-body electron-phonon-impurity supercollisions (SC), which is the main cooling mechanism at room temperature[1–4]. The case of high-mobility graphene, in spite of its technological interest, has been less investigated. The suppression of supercollisions and the vanishing of Wiedemann-Franz heat conduction at current saturation give rise to strongly out-of-equilibrium electron distributions where new cooling pathways become prominent. Intrinsic optical phonon (OP) cooling was reported in suspended graphene[5,6]. In supported graphene the coupling to remote polar phonons overwhelms that to OPs[7–11]. The case of graphene on boron nitride (GoBN) is emblematic. Firstly, current saturation can be achieved at low fields $\mathcal{E}$[12] opening access to the Zener Klein tunneling (ZKT) regime at high field[13,14]. Secondly, h-BN is a uniaxial dielectric that sustains hyperbolic phonon-polaritons (HPPs)[15–21] in the two Reststrahlen (RS) bands $\hbar\Omega_I$ = 97–103 meV and $\hbar\Omega_{II}$ = 170–200 meV. As a marked difference with SiO_2 surface modes, HPPs can efficiently radiate energy across the dielectric layer[16], avoiding hot-phonon effects and making an efficient thermal bridge between the graphene channel and the metallic gate in nanodevices.

By means of sensitive noise thermometry, we show strong evidence for a new and ultra-

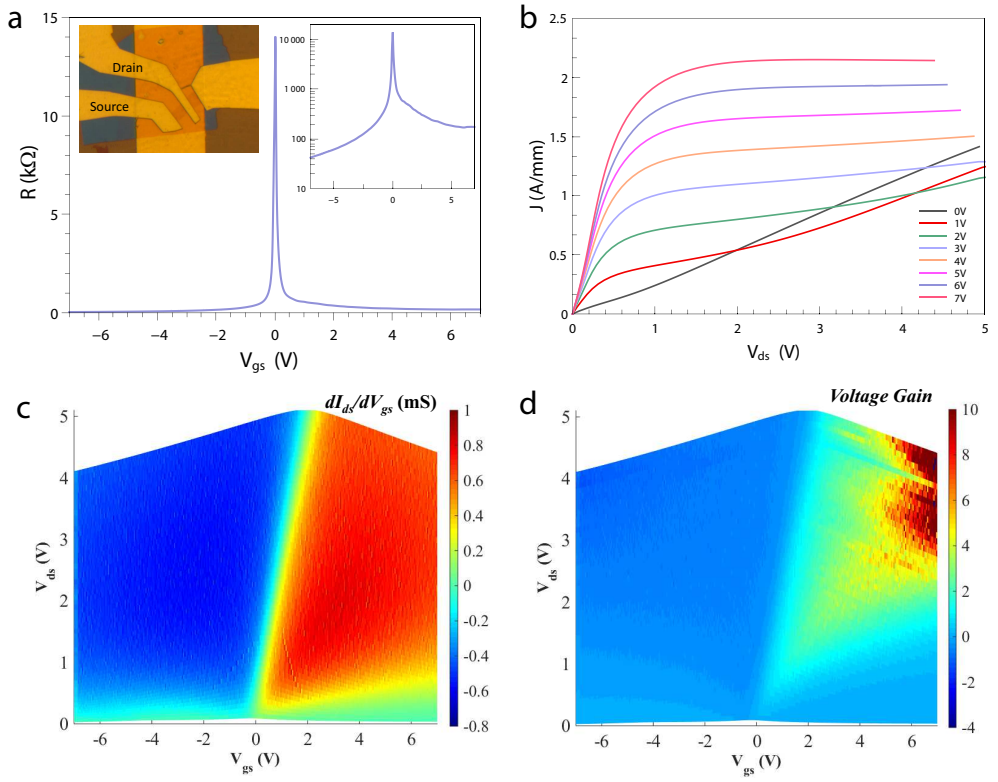

FIG. 1: Bottom-gated bilayer graphene on hBN transistor (optical image in panel a-inset). a) Low-bias transfer curve $R = 1/g_{ds}$ measured at 4 Kelvin and $V_{ds} = 10$ mV. A logarithmic plot (inset) shows the small contact resistance in the hole side and a larger one in the electron-side due to contact doping. The bilayer nature of the sample and the gate capacitance $C_g = 1.15$ mS/m^2 are deduced from independent quantum Hall measurements (not shown), from which we infer a mobility $\mu \simeq 3.10^4 \mathrm{cm}^2\mathrm{V}^{-1}\mathrm{s}^{-1}$. b) current saturation for different gate voltages in the electron doped regime (positive bias). c), d), transconductance $g_m = \partial I/\partial V_{gs}|_{V_{ds}}$ and voltage gain $G = g_m/g_{ds}$ as a function of gate and drain voltages. g_m saturates at ± 0.8 mS and changes sign along the line $V_{gs} \simeq 0.4 V_{ds}$. The gain peaks at large values ($G \simeq 10$) at high bias and high doping ($V_{ds}, V_{gs} \geq 4$ V).

efficient cooling pathway beyond the super-Plankian regime that clips the electron temperature when the ZKT threshold field is reached. This new regime suggests the emission of HPP by out-of-equilibrium electron-hole pairs.

We have investigated single layer (SLG), bilayer (BLG) and trilayer (TLG) graphene transistors where similar results are observed (see SI). However, we focus here on the BLG sample which is most illustrative essentially due to its energy independent density of states (DOS). In addition, this BLG sample approaches the intrinsic limit with $v_{sat} \simeq 3.10^5 \mathrm{m.s}^{-1}$,

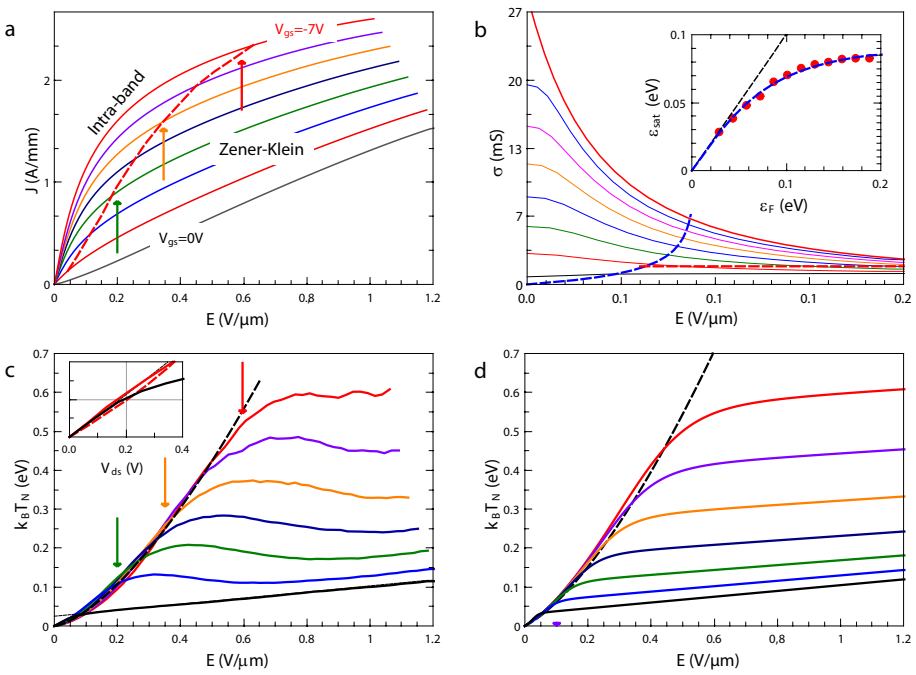

FIG. 2: **a)**: Non-linear current-field characteristics of the BLG on hBN transistor in the hole doped regime. The gate voltage (and hence carrier density and Fermi energy) increases linearly in the range $V_{gs} = [-0, -7]$ V, $p = [0, 5] \times 10^{12}$ cm^{-2} and $|\varepsilon_F| = [0, 0.2]$ eV. The onset field for Zener-Klein tunneling $\mathcal{E}_{zk}$ (see main text) is shown as a red dashed line in the plot. **b)**: Low field dependence of the differential conductivity. Blue dashed line : saturation field $\mathcal{E}_{sat}$, corresponding to $J = J_{sat}/2$ and $\sigma(\mathcal{E}) = \sigma(0)/4$. Note that the ZKT onset field (red dashed line) fulfills $\mathcal{E}_{zk}/\mathcal{E}_{sat} > 1$. Inset : Fermi energy dependence of the saturation energy ε_{sat} (defined in the text) and its fitting to $\varepsilon_{sat} = (\varepsilon_F^{-2} + (\hbar\Omega_{sat})^{-2})^{-1/2}$ with $\hbar\Omega_{sat} = 95 \pm 5$ meV. **c)**: Bias field dependence of the noise temperature T_N. Two regimes are observed, a steep increase at low field followed by a quasi-saturation above a doping dependent threshold $V_{on} = \mathcal{E}_{on}L$. At zero doping $V_{on} \simeq 0.2$ V $\simeq \hbar\Omega_{II}$, the HPP phonon energy (inset). **d)**: Calculated $k_B T_N(V_{ds})$ plots using the heuristic model described in the text, including WF cooling at low field and out-of-equilibrium HPP emission at high field.

thereby bringing a more direct insight into the ultimate relaxation mechanisms.

A picture of the BLG transistor and its low-bias resistance are shown in Figure 1-a. The device is made of a ($L \times W = 4 \times 3$ μm), high-mobility ($\mu \simeq 3.10^4$ cm^{2}V^{-1}s^{-1}) BLG flake exfoliated on a 23 nm-thick hBN crystal deposited on a metallic (Au) bottom gate. The gate capacitance $C_{gs} \simeq 1.15$ mF/m^2 was calibrated against quantum Hall plateaus.

It mainly arises from the hBN dielectric capacitance ($\epsilon_r \simeq 3.2$) with a negligible serial quantum capacitance correction $C_Q = e^2 DOS = 2e^2 m^*/(\pi\hbar^2) \simeq 40$ mF/m^2 (effective mass $m^* \simeq 0.03\, m_0$), which defines the accessible Fermi energy range $\varepsilon_F = \frac{C_g}{C_Q} eV_g = \pm 0.2$ eV.

As seen in Figure 1-b, the device demonstrates full current saturation at moderate and high doping, whereas the emergence of a doping independent constant-resistance regime at low doping is the fingerprint of Zener-Klein tunneling of conductivity σ_{zk}[14]. The transconductance and voltage gain are shown in Figs.1-c and d. Transconductance saturates at $g_m = \pm 250$ mS/mm and voltage gain peaks at $G \simeq 10$ at large bias[12]. These figures show that this sample reaches the ultimate performances allowed by the intrinsic properties of graphene. As seen in Fig.1-c, the transconductance vanishes along a line $V_g \simeq 0.4 V_d$ (charge neutrality in the channel) reflecting a geometrical correction due to the near vicinity of the gate electrode. From that line we deduce the average channel doping, $ne = C_{gs}V_{gs} + C_{gd}V_{gd} \simeq C_g(V_{gs} - 0.4V_{ds})$. The full current saturation at higher doping in Fig.1-b actually results, with a differential conductivity $\sigma = \sigma_{zk} - C_{gd} v_{sat} L \simeq 0$ in our 4 μm-long samples, from the balance of the ZKT current by a decrease of the intraband saturation current due to the pinching of the carrier density when increasing V_{ds} at constant V_{gs} at the electron side.

In Fig.2-a we have corrected for drain doping by biasing along constant density lines, $V_{gs} - 0.4V_{ds} = Const$, and we work in the p-doped regime where contact resistance is minimized (see inset of Figure 1-a), presumably due to efficient contact gating[24]. Similar results are obtained in the electron doped regime[39]. Fig.2-a shows the full current-bias characteristics measured at constant carrier densities as explained above. Those are consistent with previous investigations[9,10,12,22,23,25] although the higher mobility of our sample makes it possible to gain a deeper insight into the ZKT regime.

At low fields, we observe a strong increase of the intraband current with doping (up to 2 A/mm at a hole density $p = 5.10^{12}$ cm^{-2}). Due to the high mobility, the current density rapidly reaches important values and saturates. Fig.2-b shows the differential conductance σ at low-field where the ZKT contribution is limited and intraband transport dominates. It obeys a $\sigma(\mathcal{E}) = \sigma(0)/(1 + \mathcal{E}/\mathcal{E}_{sat})^2$ dependence[12] corresponding to a current density $J(\mathcal{E}) = J_{sat}\mathcal{E}/(\mathcal{E} + \mathcal{E}_{sat})$ where $\mathcal{E}_{sat}$ is the saturation electric field. From the doping dependence of $\sigma(0)$, we extract a finite field mobility $\mu \simeq 2.8$ m^{2}V^{-1}s^{-1} consistent with the zero field measurement (Fig 1-a). From $\mathcal{E}_{sat}$, sketched as a blue dashed line in Fig.2-b, we define a

saturation velocity $v_{sat} = \mu\mathcal{E}_{sat} = J_{sat}/ne$ and a saturation energy $\varepsilon_{sat} = \frac{\pi}{2}\hbar k_F {v_{sat}}$[9], which is plotted in Fig.2-b (inset). At low doping the saturation energy is limited by the Fermi energy (channel saturation). The saturation of ε_{sat} at high doping is generally attributed to OP (or remote phonon) scattering (energy $\hbar\Omega$), according to[9] $\varepsilon_{sat} = \hbar\Omega$. Both the linear increase $\varepsilon_{sat} \propto |\varepsilon_F|$ and the trend to saturation are observed. We extract the asymptotic limit by fitting the data to the empirical formula $\varepsilon_{sat} = (\varepsilon_F^{-2} + (\hbar\Omega_{sat})^{-2})^{-1/2}$. We deduce $\hbar\Omega_{sat} \simeq 95 \pm 5$ meV which is consistent with remote phonons $\hbar\Omega_I$ of the lower RS band of h-BN.

At higher bias, interband (ZKT) transport takes over, leading to a constant differential conductance $\sigma_{zk} \simeq 1$ mS. Similar behavior is observed in SLG and TLG devices with $\sigma_{zk}^{SLG} \simeq 1.2$ mS and $\sigma_{zk}^{TLG} \simeq 2$ mS. In analogy with Klein tunneling in abrupt p-n junctions in graphene[26], ZKT is constrained by energy/momentum conservation[14] which sets a threshold field at $\mathcal{E}_{zk} = 2\varepsilon_F/(el_{zk})$, where l_{zk} is the doping-dependent tunneling length. ZKT bears strong analogies with optical pumping as it involves vertical interband transitions (bound by Pauli blocking) with electron-hole pair creation at a rate $\dot{n}_{e-h} = ek_F/(\hbar\pi^2)(\mathcal{E} - \mathcal{E}_{\mathcal{ZK}})$. As a marked difference, the pumping energy window increases linearly with the applied field $\mathcal{E} - \mathcal{E}_{zk}$. In the absence of theoretical prediction for BLG-ZKT, we rely on the transmission of a sharp BLG p-n junction[26], $D = k_F W/4\pi$ to deduce the ZKT conductance. To account for the finite length effect of the junction, we introduce a transparency factor $\alpha_{zk} \simeq 0.3$ (deduced from the noise measurements, see below). Thus, the ZKT conductance reads $\sigma_{zk} = \alpha_{zk}\ \frac{4e^2}{h}\ (k_F l_{zk})/4\pi$. In this simple picture, a doping and field independent ZKT conductivity translates into a constant $\alpha_{zk}k_F l_{zk}$ that we deduce from the low-doping data where the ZKT regime is prominent. We are thus able to compute the threshold field $\mathcal{E}_{zk} = 2|\varepsilon_F|/(el_{zk})$ for each carrier density (red dashed line in Fig.2-a). The main outcome of our current-bias analysis is that in quasi intrinsic samples intraband current saturation and Zener-Klein tunneling have different onset fields (blue and red lines in Fig. 2-b), especially at large doping, $|\varepsilon_F| = 200$ meV, where $\mathcal{E}_{sat} \simeq 90$ mV/μm and $\mathcal{E}_{zk} \simeq 500$ mV/μm.

Noise thermometry, combined with Joule heating, is a powerful tool to investigate energy relaxation[27–30]. It relies on the measurement of current noise power density $S_I(f)$ at a frequency large enough to exceed the $1/f$ noise corner frequency which increases with bias. The noise temperature (equal to the electron temperature in quasi-equilibrium situations) is experimentally defined as $k_B T_N = S_I(L/4\sigma W)$. Technically we have adapted our standard

setup[28,31,32] to work in the 1–10 GHz band (see SI) and accommodate the high bias conditions. Previous studies have investigated the thermalization sequence in graphene samples upon increasing power. This sequence usually starts with WF heat conduction on a limited window in diffusive samples and then displays the signatures of various electron-AC phonon coupling mechanisms[32–34] and the emergence of new mechanisms like SCs[3,4] or interaction effects with Dirac fluid behavior at low density[35]. The bottom line of these studies is the observation of power-laws $P_{cool} \propto T_e^{\beta}$ between cooling power P_{cool} and electronic temperature T_e. Fig.2-c shows the very peculiar thermal behavior of high-mobility graphene on h-BN with an abrupt switching between two cooling mechanisms and the clipping of the electronic temperature at high bias.

The low-bias mechanism is naturally WF-cooling that develops on a wide window due to the large heat conductivity $\kappa \propto \sigma$ and the absence of SCs in high-mobility graphene. It relies on solutions of the (1D) heat equation $\frac{1}{2}\mathcal{L}\sigma\partial^2 T^2/\partial x^2 = P_J$, where P_J is the Joule heating density and $\mathcal{L} = (\pi^2 k_B^2)/(3e^2)$ is the Lorenz number. Assuming uniform Joule heating and accounting for cold contacts, one gets $k_B T_N =< k_B T_e >= \mathcal{F} L e \mathcal{E}$ with the Fano factor $\mathcal{F} = \frac{\sqrt{3}}{8}$. Experimentally, the temperature shows a superlinear $T_N(V_{ds})$ behavior (Fig.2-c) that can be explained by the current saturation discussed above and the related increase of the differential conductance $\sigma(\mathcal{E})$ (Fig.2-b). The $T_N \propto \sqrt{\mathcal{E} \cdot J/\sigma}$ scaling in Fig.3-b confirms the WF nature of cooling at low bias. Taking $\mathcal{F} = 0.1$ (see below) and $\mathcal{E}_{sat} = 90$ mV/μm we can reproduce the superlinear law with $k_B T_N = \mathcal{F} L \mathcal{E} \sqrt{1 + \mathcal{E}/\mathcal{E}_{sat}}$ (Fig.2-c,d dotted lines). Note that $T_N \propto L$ in the WF regime so that smaller thermal energy scales would be observed in shorter samples.

As seen in Fig.2-c the noise temperature deviates from the WF cooling limit above a doping dependent onset voltage $V_{on} = L\mathcal{E}_{zk}$ and saturates at large electric field (and Joule power) indicating a very efficient cooling mechanism, pointing to a direct coupling of electrons to substrate polar modes[7]. A crucial difference between the low-bias and high-bias cooling mechanisms lies in their opposite dependence on carrier concentration as shown in Fig. 3-a. The usual observation -the larger the carrier density, the lower the electron temperature- which holds for most cooling mechanisms reported so far (including ACs, SCs, OPS, or WF[3,36]) breaks down for the high-bias regime. The existence of plateaus, and the increase of the plateau-temperature with doping, point to the onset of a new cooling mechanism driven by Pauli blocking (see arrows in Fig.2-a and c). A second hint on this cooling

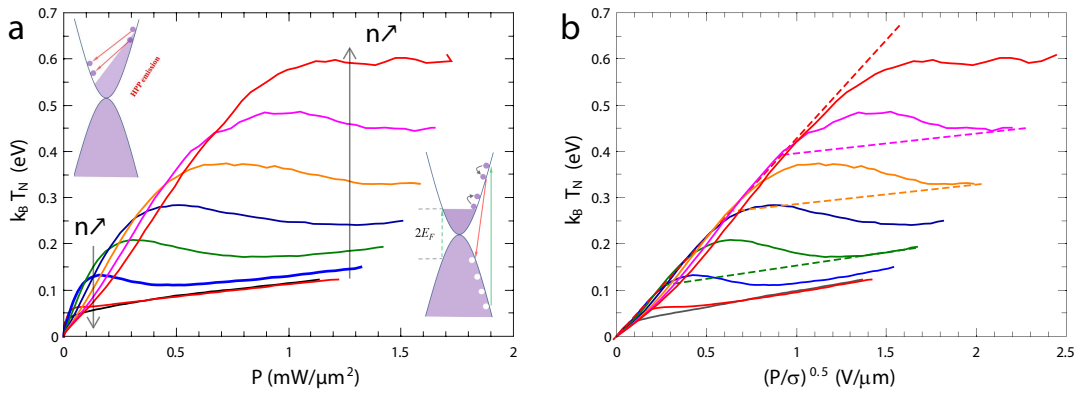

FIG. 3: (a) Noise temperature as a function of the Joule heating. The sketches represent the dominating cooling processes : intra-band electron-electron interactions at low field and interband HPP emission at high field. (b) Wiedemann-Franz scaling of the noise temperature data; from the subthreshold slope we deduce the Fano factor $\mathcal{F} \simeq 0.105$ and a residual slope $\mathcal{F} \simeq 0.015$ above the threshold.

process is given by the lower limit $V_{on} \sim 0.2$ V at neutrality (inset). This feature, also seen in the SLG and TLG noise data (SI), points to an activation energy close to the second RS band of BN, $\hbar\Omega_{II} \simeq 0.2$ eV.

In isotropic polar materials, OPs are responsible for a RestStrahlen band (RS) in which light propagation is forbidden. Nevertheless, surface modes polaritons (SPhPs) can develop which create a near-field in the vicinity of the interfaces, to which the electrons of graphene can efficiently couple. The strong unixial character of hBN is responsible for the splitting of the RS band into a lower out-of-plane band (97-100 meV) and a higher in-plane band (170-200 meV). In these RS bands, where each mode brings a dielectric function with real parts of opposite signs, the usual evanescent SPhPs are replaced by propagating hyperbolic phonon polariton (HPP) modes[19]. The large number of HPP modes (the number of branches equals the number of BN layers) strongly enhances the cooling capability of HPPs compared to SPhP. Furthermore, while the vertical transport of energy by SPhPs is limited to their evanescent decay length (about 1nm in our situation), energy transport by HPPs in only limited by their anharmonic decay which leads to characteristic depths of 30 nm. In our device, the efficient coupling to the hBN layer opens up thermal pathways reaching the gold backgate where heat is efficiently drained away from the transistor (inset of Fig. 4-a).

In this context, heat transfer from the graphene layer to the hBN substrate can be seen as

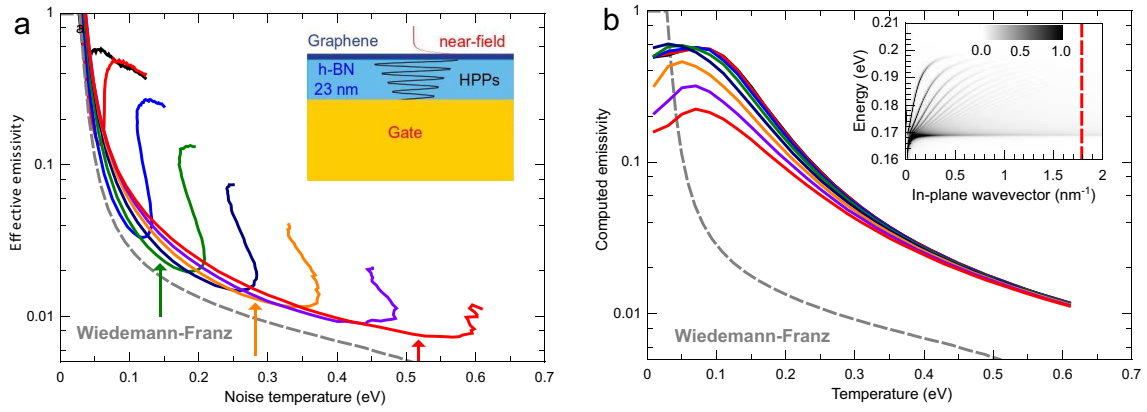

FIG. 4: (a) Experimental emissivity computed as the ratio of the Joule power to the theoretical super-Planckian power. The blue region represents the WF backgound whereas the light blue area highlights the HPP cooling contribution in the intermediate temperature regime. Inset : Sketch of the radiative heat transfer by HPPs. (b) Theoretical emissivity of the BLG-hBN(23 nm)-Au stack computed as a function of the temperature of the graphene electrons for a BLG in the local approximation. Inset : Monochromatic emissivity $M(\omega, k)$ of the BLG/hBN/Au stack, showing strong Fabry-Perot-like resonances in the 23 nm-thick hBN layer. Dashed line : Wavevector cut-off $k_c(\omega, E_F, T)$ used for the calculation of the super-Planckian radiated power. The emissivity of the main panel is the frequency and wavevector average of $M(\omega, k)$ over the whole RS band.

black-body radiation into a material bearing specific hyperbolic modes. In vacuum, black-body radiation in the far field is strongly constrained by the light cone ($k_\parallel \leq k_0 = \omega/c$) that puts severe restrictions on the momentum exchange. This picture has to be revisited when the distance between the black-body and the dielectric becomes shorter than the thermal wavelength $\lambda_T = \hbar c/k_B T$, reaching the so-called super-Planckian regime where thermal coupling mainly occurs through evanescent modes[37] up to a wavevector $1/d$. The thermal contact is reached when $d \lesssim \lambda_F$ as the momentum exchange becomes limited by the electron wavevectors.

Real bodies are characterized by their emissivity $M(\omega)$, that is their relative radiative efficiency compared to the black-body emission. Fig. 4-a represents the experimental average emissivity M of our device as a function of the temperature, which is the ratio of the Joule power to the maximum theoretical super-Planckian radiation power of the BLG on the

hBN slab (see SI). If super-Planckian radiation was the main thermal channel, a smoothly decreasing emissivity would be observed as calculated in Fig. 4-b. In contrast, experimental data show a strong deviation for both the low and high temperature sides. The apparently diverging emissivity below $k_BT = 40$ meV is an artefact due to the increasing contribution of the WF cooling at low T. Above $k_BT = 90$ meV, the super-Planckian HPP emissivity becomes significant and scales similarly to WF cooling. This contribution of HPP cooling in the intermediate temperature regime (40 meV $< k_BT < E_F$) accounts for the reduced Fano factor $\mathcal{F} \simeq 0.1$ reported consistently in hBN supported graphene samples.

The most striking feature in Fig. 4-a is a sudden jump of the emissivity at a doping dependent temperature threshold. This behavior cannot be understood within a thermal scheme since the emissivity at fixed doping should only show a smooth dependence with temperature. This dramatic increase of the emissivity by more than a decade shows that an ultra efficient, strongly off-equilibrium process sets in. Interestingly, this new thermal channel arises concomitantly with the switch of the transistor in the ZKT regime (Fig. 2-a and b) that is equivalent to an electrical pumping of electron-hole pairs. Thus, we speculate that this thermal channel is due to the emission of HPPs from an inverted electron-hole pair population. In this respect, the threshold voltage ($V_{ds} \simeq 0.2$ V) near neutrality shows that e-h pairs generated by ZKT with an energy below $\hbar\Omega_{II}$ are naturally unable to cool the sample. In total, noise thermometry allows to conclude that beyond a first regime which is most probably thermal, HPP emission above the ZKT onset field is a highly out-of-equilibrium process.

The temperature plateaus observed at high doping when cranking up the bias above the ZKT threshold show that the off-equilibrium emission of HPPs yields a cooling power P_{HPP} that exactly compensates the excess Joule power ΔP_J: $\Delta P_J = P_{HPP}$. In the saturation regime and neglecting the small ZKT current, the excess Joule power reads $\Delta P_J \simeq J_{sat}(\mathcal{E} - \mathcal{E}_{ZK}) = 2\varepsilon_{sat} e k_F/(\pi^2\hbar) \times (\mathcal{E} - \mathcal{E}_{ZK})$, whereas the power drained away by HPP emission reads $P_{HPP} = \dot{n}_{e-h}\hbar\Omega_{II}$ with, for e-h pairs created by ZKT, $\dot{n}_{e-h} = e k_F/(\hbar\pi^2)(\mathcal{E} - \mathcal{E}_{ZK})$. Obviously, those powers equilibrate provided that $2\varepsilon_{sat} = \hbar\Omega_{II}$, which is roughly the case in hBN because $\varepsilon_{sat} \simeq \hbar\Omega_I \simeq \hbar\Omega_{II}/2$. Interestingly, this observation shows that in quasi-intrinsic samples, the temperature saturation at high doping ultimately arises from the peculiar frequencies of the hBN RS bands. Taking this effect into account together with the nonlinear WF cooling described above, we have plotted in Fig.2-d a simulation of the noise

temperature as a function of bias voltage using $\alpha_{zk} = 0.3$ as a free parameters and $\mathcal{F} = 0.1$ from the WF scaling in Fig.2-e. The agreement with experiment is good and supports our heuristic model, in particular our main hypothesis that HPP cooling can fully compensate Joule heating so that electronic temperature itself is clipped. Furthermore, we anticipate that in diffusive samples, the lower saturation current (and thus lower Joule power) would lead to a lower equilibrium temperature.

In order to characterize further the non-equilibrium HPP emission, it is enlightening to estimate the steady density of electron-hole pairs in the ZKT regime. In fact, for non-thermal electron distributions, the noise temperature T_N has an additional contribution above T_e that is directly related to the presence of non-equilibrium holes. Owing to the constant DOS in BLG, this correction can be captured by splitting the noise temperature integral along the conduction and valence bands and writing, for an electron doped BLG, $k_B T_N \simeq k_B T_e + n_{e-h}/DOS$ with $k_B T_e \simeq \int_0^\infty f(1-f)dE$ and $n_{e-h} = \int_{-\infty}^0 DOS(1-f)dE$ as $f(E<0) \lesssim 1$ in weak ZK tunneling conditions. This correction set the absolute noise floor for a cold BLG ZKT transistor at $k_B T_N = 2n_{e-h}/DOS$. In the steady state, the recombination of e-h pairs into HPPs at a rate $\dot{n}_{e-h} = -n_{e-h}/\tau$ (where τ is an effective HPP emission time) just equilibrates the e-h generation by ZKT. We thus obtain $n_{e-h} = 2\tau\sigma_{zk}/el_{zk} \times (\mathcal{E} - \mathcal{E}_{zk})$ consistent with the residual linear dependence $T_N(\mathcal{E})$ observed in the low-doping limit where the ZKT regime is most developed (Fig. 2-c). The slope of $T_N(\mathcal{E})$ near neutrality yields $\tau \simeq 0.5$ ps. Note that the emission time τ is much larger that the intraband electron-electron relaxation time ($\simeq 50$ ps)[38] but roughly 5 times smaller than the intrinsic OP emission time[7]. This provides a consistent picture of the cooling pathway where electrons in the conduction band rapidly thermalize with the Fermi sea, whereas intrinsic energy relaxation by OPs is quenched by a much faster coupling to HPPs.

In conclusion, using combined transport and noise thermometry we have shown that quasi-intrinsic bilayer graphene on hBN transistors have remarkable thermal properties, dominated by Wiedeman-Franz conduction and hBN hyperbolic phonon polariton emission. In particular, we have unveiled a new off-equilibrium HPP emission process subsequent to the generation of electron-hole pairs by Zener-Klein tunneling, which yields to the temperature plateaus observed at high doping. A direct signature of this non-equilibrium hole population is observable as a linear correction to the electronic temperature in the noise power in the low-doping limit. This GoBN technology based on local gating of high mobility graphene

through a thin hBN layer opens up many perspectives : in terms of applications it makes up a promising platform for RF power amplification and for the design of original cooling pathways in nano-devices; in terms of basic science it opens up the study of cold cooling pathways involving off-equilibrium carrier generated by tunneling processes, and promotes graphene as dedicated IR-photon source for HPP optics.

Acknowledgments

The research leading to these results have received partial funding from the European union Seventh Framework programme under grant N:604391 Graphene Flagship, and from the ANR-14-CE08-018-05 "GoBN". G.Z. acknowledges the financial supports from the National Basic Research Program of China (973 Program) under the grant No. 2013CB934500, the National Science Foundation of China (NSFC) under the grant No. 61325021.

Author contributions WY, EB, CV and BP conceived the experiment and developed the models. WY, SB conducted the measurements. AD designed the sample holder. WY, XL, MR, TT, KW, GZ participated to sample fabrication. WY, SB, GF, JMB, EB, CV and BP participated to the data analysis. WY, EB, CV and BP wrote the manuscript with contributions from the coauthors.

Additional information Competing financial interests: The authors declare no competing financial interests.

---

* Electronic address: bernard.placais@lpa.ens.fr

[1] J. C. W. Song, M. Y. Reizer, and L. S. Levitov, *Phys. Rev. Lett.* **109**, 106602 (2012). *Disorder-assisted electron-phonon scattering and cooling pathways in graphene.*

[2] M. Graham, S.-F. Shi, D. C. Ralph, J. Park, and P. L. McEuen, *Nat. Phys.* **9**, 103 (2013). *Photocurrent measurements of supercollision cooling in graphene*

[3] A.C. Betz, S.H., Jhang, E. Pallecchi, R. Feirrera, G. Fève, J-M. Berroir, B. Plaçais, *Nat. Phys.* **9**, 109 (2013). *Supercollision cooling in undoped graphene.*

[4] A. Laitinen, M. Oksanen, A. Fay, D. Cox, M. Tomi, P. Virtanen, and P.J. Hakonen. *Nano Lett.* **14**, 3009 (2014). *Electron phonon coupling in suspended graphene: supercollisions by ripples.*

[5] B. Gao, G. Hartland, T. Fang, M. Kelly, D. Jena, H. Xing, L. Huang, *Nano Lett.* **11**, 3184 (2011). *Studies of Intrinsic Hot Phonon Dynamics in Suspended Graphene by Transient Absorption Microscopy*

[6] A. Laitinen, M. Kumari, M. Oksanen, B. Plaçais, P. Virtanen, and P.J. Hakonen. *Phys. Rev. B* **91**, 121414 (R) (2014). *Electron-optical phonon coupling in suspended graphene bilayer.*

[7] T. Low, V. Perebeinos, R. Kim, M. Freitag and P. Avouris *Phys. Rev. B* **86**, 045413 (2012). *Cooling of photoexcited carriers in graphene by internal and substrate phonons.*

[8] J. K. Viljas, T.T. Heikkilä, *Phys. Rev. B* **81**, 245404 (2010). *Electron-phonon heat transfer in monolayer and bilayer graphene.*

[9] A. Barreiro, M. Lazzeri, J. Moser, F. Mauri, A. Bachtold, *Phys. Rev. Lett.* **103**, 076601 (2009). *Transport Properties of Graphene in the High-Current Limit*

[10] A.M. DaSilva, K. Zou, J.K. Jain, J. Zhu, *Phys. Rev. Lett.* **104**, 236601 (2010). *Mechanism for Current Saturation and Energy Dissipation in Graphene Transistors*

[11] L. Huang, B. Gao, G. Hartland, M. Kelly, H. Xing, *Surf. Science* **605**, 1657 (2011). *Ultrafast relaxation of hot optical phonons in monolayer and multilayer graphene on different substrates*

[12] N. Meric, M. Y. Han, A. F. Young, B.A. Ozylmaz, P. Kim, K. L. Shepard, *Nat. Nanotech.* **3**, 654 (2008). *Current saturation in zero-bandgap, topgated graphene field-effect transistors*

[13] N. Vandecasteele, A. Barreiro, M. Lazzeri, A. Bachtold, F. Mauri, *Phys. Rev. B* **82**, 045416 (2010). *Current-voltage characteristics of graphene devices: Interplay between Zener-Klein tunneling and defects*

[14] G. Kane, M. Lazzeri, F. Mauri, *J. Phys.: Condens. Matter* **27**, 164205 (2015). *High-field transport in graphene: the impact of Zener tunneling*

[15] Y. Guo, C.L. Cortes, S. Molesky, Z. Jacob, *App. Phys. Lett.* **101**,131106 (2012) *Broadband super-Planckian thermal emission from hyperbolic metamaterials*

[16] S.-A. Biehs, M. Tschikin, P. Ben-Abdallah, *Phys. Rev. Lett.* **109**, 104301 (2012) *Hyperbolic Metamaterials as an Analog of a Blackbody in the Near Field*

[17] S.-A. Biehs, M. Tschikin, R. Messina, P. Ben-Abdallah, *App. Phys. Lett.* **105**,161902 (2014). *Super-Planckian far-zone thermal emission from asymmetric hyperbolic metamaterials*

[18] S. Dai, Q. Ma, M. K. Liu, T. Andersen, Z. Fei, M. D. Goldflam, M. Wagner, K. Watanabe, T. Taniguchi, M. Thiemens, F. Keilmann, G. C. A. M. Janssen, S-E. Zhu, P. Jarillo-Herrero, M. M. Fogler, D. N. Basov, *Nat. Nanotech.* **10**, 682 (2015). *Graphene on hexagonal boron nitride*

as a tunable hyperbolic metamaterial

[19] A. Kumar, T. Low, K. H. Fung, P. Avouris, N. X. Fang, *Nano Lett.* **15**, 3172 (2015). *Tunable Light-Matter Interaction and the Role of Hyperbolicity in Graphene-hBN System*

[20] A.J. Giles,S. Dai,J. Glembocki,A.V. Kretinin,Z.Sun, C.T. Ellis,J.G. Tischler,T. Taniguchi,K. Watanabe, M.M. Fogler,K.S. Novoselov,D.N. Basov, J.D. Caldwell, *Nano Lett.* **16**, 3858 (2016) *Imaging of Anomalous Internal Reflections of Hyperbolic Phonon-Polaritons in Hexagonal Boron Nitride*

[21] A. Principi, M. B. Lundeberg, N.C.H. Hesp, K-J. Tielrooij, F.H.L. Koppens, M.Polini, *arXiv:1608.01516v1 Super-Planckian electron cooling in a van der Waals stack*

[22] M. Freitag, M. Steiner, Y. Martin, V. Perebeinos, Z. Chen, J.C. Tsang, P. Avouris, *Nano Lett.* **9**, 1883 (2009). *Energy Dissipation in Graphene Field-Effect Transistors*

[23] V. Perebeinos, P. Avouris, *Phys. Rev. B* **81**, 195442 (2010). *Inelastic scattering and current saturation in graphene*

[24] Q. Wilmart, A. Inhofer, M. Boukhicha, W. Yang, M. Rosticher, P. Morfin, N. Garroum, G. Fve, J.-M. Berroir, B. Plaais *Scientific Reports* **6**, 21085 (2016). *Contact gating at GHz frequency in graphene*

[25] N. Meric, C.R. Dean, N. Petrone, J. Hone, P. Kim, K. L. Shepard, *Proc. IEEE* **101**, 1609 (2013). *Graphene Field-Effect Transistors Based on BoronNitride Dielectrics*

[26] M. I. Katsnelson, K. S. Novoselov, A. K. Geim, *Nat. Phys.* **2**, 620 (2006). *Chiral tunnelling and the Klein paradox in graphene*

[27] F. Wu, P. Queipo, A. Nasibulin, T. Tsuneta, T. H. Wang, E. Kauppinen, and P. J. Hakonen, *Phys. Rev. Lett.* **99**, 156803 (2007). *Shot Noise with Interaction Effects in Single-Walled Carbon Nanotubes*

[28] J. Chaste, E. Pallecchi, P. Morfin, G. Fève, T. Kontos, J.-M. Berroir, P. Hakonen, B Plaçais, *Appl. Phys. Lett.* **96**, 192103 (2010). *Thermal shot noise in top-gated single carbon nanotube field effect transistors*

[29] D.F. Santavicca, J.D. Chudow, D.E. Prober, M.S. Purewal, P. Kim, *Nano Lett.* **10**, 4538 (2010). *Energy Loss of the Electron System in Individual Single-Walled Carbon Nanotubes*

[30] C. Voisin, B. Plaçais, *J. Phys.: Condens. Matter* **27**, 160301 (2015). *Hot carriers in graphene*

[31] D. Brunel, S. Berthou, R. Parret, F. Vialla, P. Morfin, Q. Wilmart, G. Fève, J-M. Berroir, P. Roussignol, C. Voisin, B. Plaçais, *J. Phys.: Condens. Matter* **27**, 164208 (2015). *Onset of*

optical-phonon cooling in multilayer graphene revealed by RF noise and black-body radiation thermometries

[32] A.C. Betz, F. Vialla, D. Brunel, C. Voisin, M. Picher, A. Cavanna, A. Madouri, G. Fève, J-M. Berroir, B. Plaçais, E. Pallecchi, *Phys. Rev. Lett.* **109**, 056805 (2012). *Hot electron cooling by acoustic phonons in graphene.*

[33] C.B. McKitterick, D.E. Prober, M. J. Rooks, *Phys. Rev. B* **93**, 075410 (2016). *Electron-phonon cooling in large monolayer graphene devices*

[34] K.C. Fong, E. E. Wollman, H. Ravi, W. Chen, A. A. Clerk, M. D. Shaw, H. G. Leduc, K. C. Schwab, *Phys. Rev. X* **3**, 041008 (2013). *Measurement of the Electronic Thermal Conductance Channels and Heat Capacity of Graphene at Low Temperature*

[35] J. Crossno, J.K. Shi, K. Wang, X. Liu, A. Harzheim, A. Lucas, S. Sachdev, P. Kim, T. Taniguchi, K. Watanabe, T.A. Ohki, K.C. Fong, *Science* **351**, 6277 (2016). *Observation of the Dirac fluid and the breakdown of the Wiedemann-Franz law in graphene*

[36] R. Bistritzer, A.H. MacDonald, *Phys. Rev. Lett.* **102**, 206410 (2009). *Electronic cooling in graphene.*

[37] S-A. Biehs, E. Rousseau, J-J. Greffet, *Phys. Rev. Lett.* **105**, 234301 (2010). *Electronic cooling in graphene.*

[38] D. Brida, A. Tomadin, C. Manzoni, Y. J. Kim, A. Lombardo, S. Milana, R. R. Nair, K. S. Novoselov, A. C. Ferrari, G. Cerullo, M. Polini, *Nature Commun.* **4**, 1987, (2013). *Ultrafast collinear scattering and carrier multiplication in graphene*

[39] For the sake of clarity, in the following all the qualitative discussions assume electron doping.

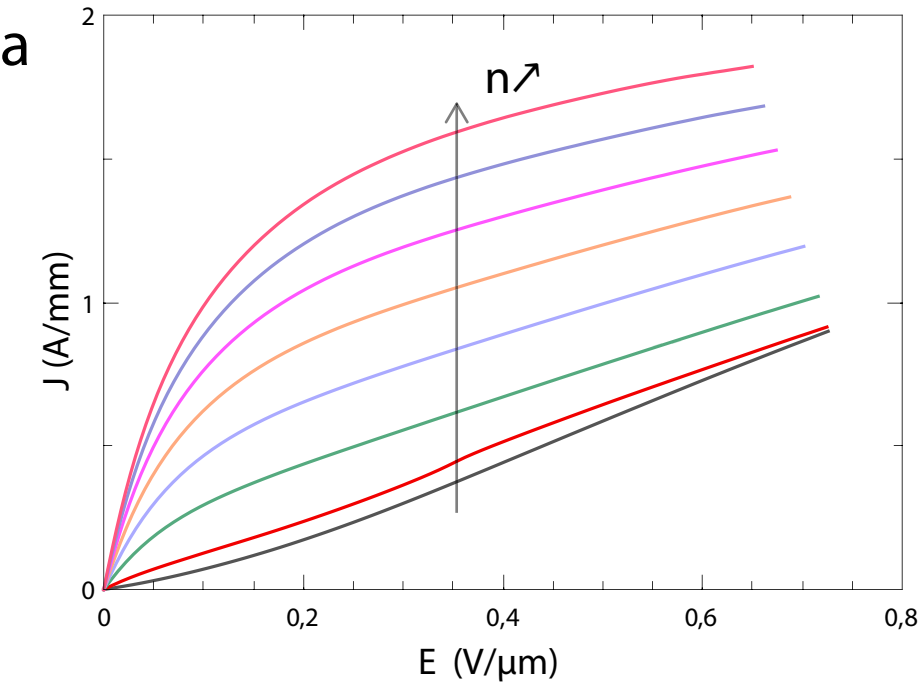
a
n↗
J (A/mm)
E (V/µm)
0
1
2
0,2
0,4
0,6
0,8

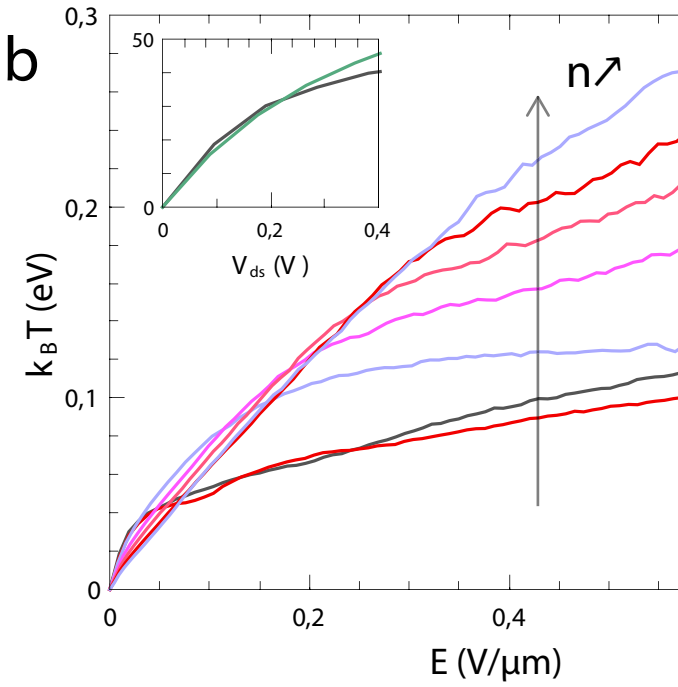
b
n↗
$k_B T$ (eV)
E (V/µm)
V_{ds} (V)
0
0,1
0,2
0,3
0,4
50

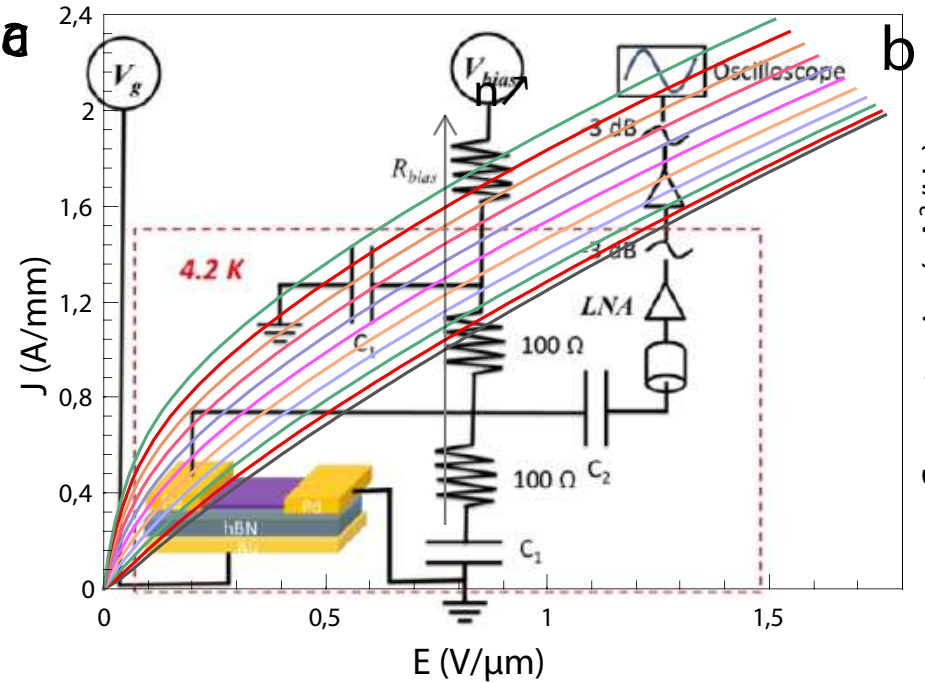
a
J (A/mm)
E (V/µm)
V_g
V_{bias}
n↗
R_{bias}
4.2 K
C_1
100 Ω
100 Ω
C_2
C_1
3 dB
3 dB
LNA
Oscilloscope
hBN
0
0,4
0,8
1,2
1,6
2
2,4
0,5
1
1,5

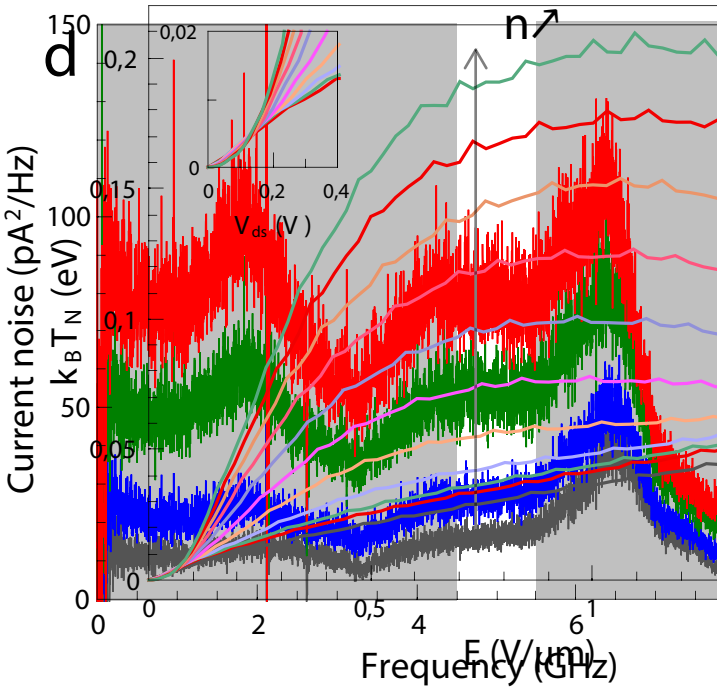
b
d
n↗
Current noise (pA²/Hz)
$k_B T_N$ (eV)
Frequency (GHz)
E (V/µm)
V_{ds} (V)
0
50
100
150
0,05
0,1
0,15
0,2
0,02
0,4
2
4
6
0,5
1